



1 **Electrical conductivity in the mantle transition zone beneath Mongol-**  
2 **Okhotsk suture: revealed by the geomagnetic signals of ground**  
3 **observatories**

4 Yanhui Zhang<sup>(1)</sup>, Yuyan Zhang<sup>(1)</sup>, Longshuang Ma<sup>(1)</sup>, Yue Yang<sup>(2\*)</sup>

5 <sup>1</sup>School of Safety Engineering and Emergency Management, Shijiazhuang Tiedao University,  
6 Shijiazhuang, 050043, China

7 <sup>2</sup>First Institute of Oceanography, Ministry of Natural Resources, Qingdao, 266061, China

8 \*Correspondence: jlyangyue@126.com

9 **Abstract:** The closure of the Mongo-Okhotsk ocean has a strong influence on the  
10 tectonic evolution of Northeast China. However, the dynamic mechanism in the  
11 Mongol-Okhotsk suture area is controversial. This paper intends to obtain the deep  
12 structure of beneath Northeast China based on geomagnetic depth sounding, and  
13 constrain the subduction of Mongol-Okhotsk Ocean from the perspective of electrical  
14 properties. This paper collects and processes the data of geomagnetic stations in China  
15 and adjacent areas, and obtains stable *C*-response data. The staggered grid finite  
16 difference method is used for forward modeling, and the finite memory quasi Newton  
17 method based on  $L_1$ -norm is used for inversion. The three-dimensional inversion of  
18 geomagnetic data is carried out in spherical coordinates. The intensive model testing  
19 stations can obtain high-resolution underground electrical structures. The measured  
20 data show that there are obvious high conductivity anomalies in the mantle transition  
21 zone in Northeast China, especially in the west of the Great Xing'an Range, showing  
22 an area of high conductivity anomalies. Combined with the regional tectonic  
23 background of the region, we speculate that the high conductivity anomaly body is  
24 related to the southward subduction of the Mongol-Okhotsk Ocean. The Mongol-  
25 Okhotsk Ocean subducted under the Eurasian plate at a small angle in the southward  
26 direction. With the closing of the Okhotsk Ocean and the extension environment after  
27 the termination of subduction, the subducted oceanic crust plate has been faulted and  
28 depressed and partially stopped in the mantle transition zone.



29 **Keywords:** Geomagnetic depth sounding; Three-dimensional inversion; Electrical structure;  
30 Mongol-Okhotsk suture; Subduction  
31

## 32 **1. Introduction**

33 It is generally believed that the tectonic evolution of Northeast China, like that of  
34 South China and North China, is affected and controlled by the westward subduction  
35 of the Western Pacific plate. However, the characteristics of other Mesozoic Cenozoic  
36 sedimentary basins and the development of volcanic rocks in Northeast China are  
37 obviously different from those in East China. It is difficult to explain these phenomena  
38 simply by controlling the activities of the ancient Pacific plate. Besides the subduction  
39 of the Western Pacific plate, the reason for this difference may also be related to its  
40 unique tectonic location.

41 Mongol-Okhotsk suture zone locates in Northeast China, which extends from  
42 central Mongolia to the Okhotsk Sea. The existence of the Paleozoic and Mesozoic  
43 Mongol-Okhotsk Sea can be clearly seen from the Mongol-Okhotsk suture. The now  
44 extinct Mongol-Okhotsk Sea is an ocean that existed in the Paleozoic (542 – 251 Ma;  
45 Gradstein et al., 2004) and Mesozoic (251 – 66 Ma), and is located between the Siberian  
46 continental block in the north and Amuria and North China continental block in the  
47 south. It is difficult to reconstruct the history, geometry and closure of this ocean due  
48 to the lack of sufficient paleomagnetic data and the sudden termination of the dispersion  
49 suture to the west. The time and manner of ocean closure are not clear, which has led  
50 to several alternative reconstructions.

51 Evidence of subduction related magmatism has been found on both sides of the  
52 Mongol-Okhotsk suture (Zorin, 1999), indicating that subduction may have occurred  
53 below the Siberian and Amurian margins, resulting in ocean closure. The  
54 paleomagnetic data of the study also shows that the sealing began in the west and ended  
55 in the east due to the coincidence of the rotation poles of the late Permian, early Triassic  
56 and late Jurassic. This is supported by intrusions and marine fossils found in the young  
57 suture from west to east (Zhao et al., 1990; Zonenshain et al., 1990; Halim et al., 1998;



58 Tomurtogo et al., 2005).

59 Previous studies focused more on the subduction of the Mongol-Okhotsk Ocean  
60 to the Siberian craton in its north. In recent years, with the development of relevant  
61 research work, some scholars gradually realized that the closure of the eastern segment  
62 of the Mongol-Okhotsk Ocean has a wide impact on the tectonic deformation and  
63 sedimentary formation in Northeast China (Tang et al., 2015). Based on the deep  
64 seismic reflection data and the geochemical data of magmatic rocks, many scholars  
65 believe that the Mongol-Okhotsk Ocean once subducted to the south (southeast), and  
66 its closure process has squeezed the entire Northeast China and even the North China  
67 Craton.

68 However, whether the Mesozoic tectonic evolution in the northern part of the  
69 Great Xing'an Range (GXAR) is controlled by the Mongolia Okhotsk tectonic domain,  
70 or by the subduction of the ancient Pacific plate, or both, is a matter of intense debate  
71 (Sun et al., 2013; Xu et al., 2013).

72 As a geophysical exploration method that can obtain the deep electrical structure  
73 of the earth, the geomagnetic depth sounding (GDS) is expected to obtain stable  
74 characteristics of the deep electrical structure of the region, and further explore the  
75 evidence of the closure and the southward subduction of the Mongol-Okhotsk Ocean,  
76 providing further constraints for solving the above controversial issues.

77 GDS method is a unique tool to obtain deep mantle conductivity by inverting *C*-  
78 responses (Kelbert et al., 2009; Munch et al., 2017; Grayver et al., 2017). Particularly,  
79 with the application of three-dimensional (3-D) global electromagnetic (EM) induction  
80 inversion method (Egbert and Kelbert, 2012) based on the mature 3-D forward in the  
81 spherical coordinate system (Uyeshima and Schultz, 2000), GDS can now be used to  
82 obtain a conductive structure closer to the real earth, thereby playing a vital role in  
83 examining the conductivity heterogeneities of the earth (Utada et al., 2009; Kelbert et  
84 al., 2009; Kuvshinov, 2012; Semenov and Kuvshinov, 2012; Püthe et al., 2015; Koch  
85 and Kuvshinov, 2015).

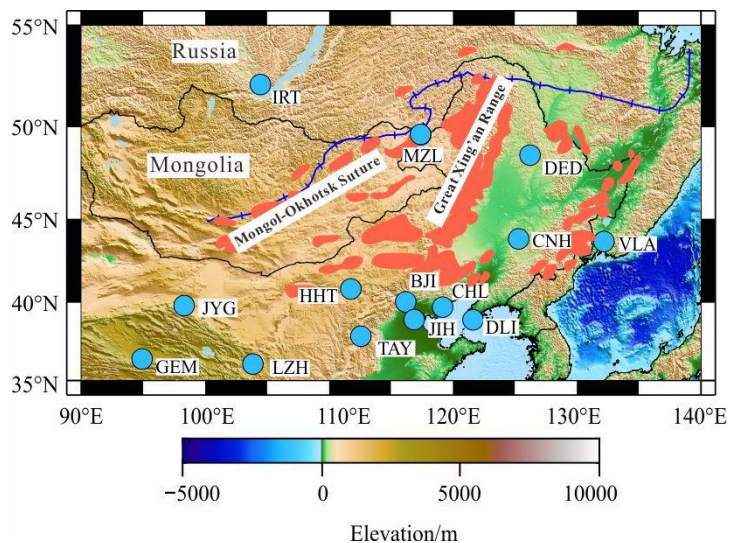
86 China has densely distributed geomagnetic observatories. However, the present



87 researches don't make full use of them, resulting in poor resolution of the electrical  
88 structure beneath China. Therefore, the existing three-dimensional (3-D) electrical  
89 conductivity models are insufficient for solving the above problems. Kelbert et al (2008)  
90 pointed out that the increase of the number of observatories can effectively improve the  
91 resolution of GDS.

92 Zhang et al (2020) proposed a data processing method which can effectively  
93 improve the utilization rate of the geomagnetic data. In addition, Li et al (2020)  
94 proposed a  $L_1$ -norm 3-D GDS inversion technology basing on the limited-memory  
95 quasi-Newton method (L-BFGS) which can greatly suppress the impact of noise data.  
96 All these provide a theoretical basis for obtaining high-precision 3-D electrical  
97 conductivity models in China.

98 In this study, more than 150 geomagnetic observatories widely distributed in China  
99 are collected, and the BIRRP software is applied for stable  $C$ -response estimation. After  
100 that, 50 high-quality response curves are obtained in and around China area. Basing on  
101 the  $L_1$ -norm 3-D inversion method, the high-precision 3-D electrical conductivity  
102 model of Northeast China is obtained. Combined with seismological and geological  
103 information, the existence of Mongol-Okhotsk Ocean and its subduction is provided  
104 with electrical constraints. Finally, the geodynamic process is discussed.





106 **Fig. 1.** Topographic map of present-day NE Asia with the locations of geomagnetic observatories  
107 and the Mongol-Okhotsk suture. Circles in blue represent the observatories, the distributions of  
108 igneous rocks are painted in orange.

## 109 **2. Method**

110 The inversion method applied in this paper is consistent with Li et al (2020), the  
111  $L_1$ -norm is used to measure data misfit which is different with the normal inversion  
112 methods.  $L_1$ -norm can effectively curb the impact of the outliers which has been  
113 approved by Farquharson (2008), more details about the inversion method can be seen  
114 at Zhang and Yang (2022).

115 The forward  $C$ -response of the corresponding model in the process of inversion  
116 should be calculated numerically. As the basis of inversion, the selection of the forward  
117 modelling method is directly related to the accuracy of inversion results. The staggered-  
118 grid finite difference method is applied in this paper, since earth is a sphere, the forward  
119 method is used in a spherical coordinate system (Uyeshima and Schultz, 2000).

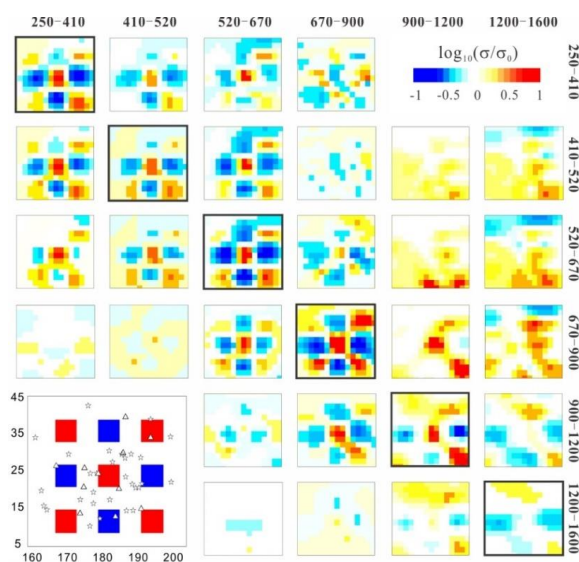
120 Different from the forward solver of Uyeshima and Schultz is the model gridding.  
121 In order to accelerate the inversion speed and try not to affect the accuracy of the  
122 inversion result, we use the local encryption method. In the research area, we will make  
123 the model mesh denser while the other region more sparsely (Li et al., 2020).

124 Most previous global electrical conductivity models are basing on the international  
125 shared geomagnetic observatories (about 11 observatories) in China (Kelbert et al.,  
126 2009; Li et al., 2020), which resulting in the low resolution of the earth models. This  
127 paper collects the densely distributed geomagnetic observatories in China and uses the  
128 data processing method based on BIRRP software (Zhang et al., 2020). Finally, 35  
129 observatories can obtain high-quality  $C$ -response in and around China area.

130 The resolution of GDS inversion under such a dense distributed observatory has  
131 been tested in the previous research by Zhang and Yang (2022). The resolution tests  
132 show that the anomalies about  $6^\circ$  at the depth of mantle transition zone and the broken  
133 stagnant plate could be detected under a relative dense spread of the geomagnetic  
134 observatories. Therefore, 3-D inversion of the observatories in and around Mongol-



135 Okhotsk suture is expected to reveal the electrical structure of the mantle transition zone,  
 136 which may could provide useful information on constraining the evolutionary process  
 137 of the Mongol-Okhotsk ocean.

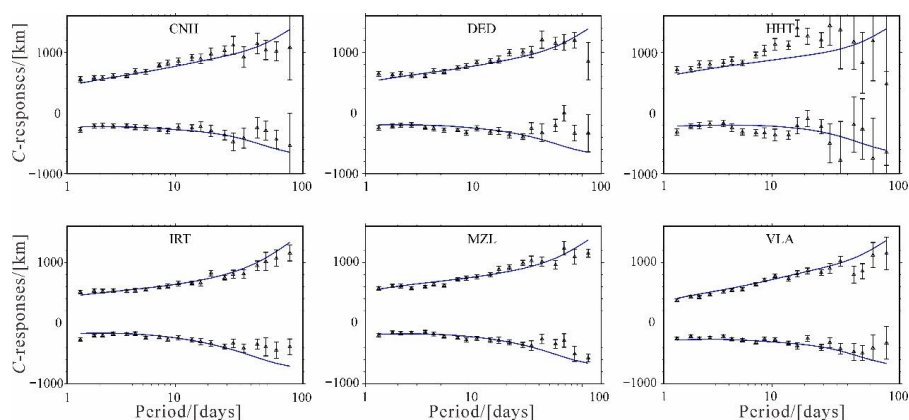


138

139 **Fig. 2.** Results of the resolution tests modified from Zhang and Yang (2022). The black boxes  
 140 are the locations of the designed anomalies; every column is an inversion result corresponding  
 141 a different layer of the anomalies, the amplitude of the anomalies is 10 times more conductive  
 142 or more resistive than the background model.

### 143 3. Real data inversion

144 Focus on the study area, 35 stable *C*-response curves of the observatories in  
 145 Northeast Asia (as shown in Fig. 1) are used for 3-D inversion. Their *C*-responses are  
 146 estimated based on the BIRRP software (Zhang et al. 2020). During inversion, the  
 147 background model is a 12-layer global mean conductivity model which is obtained by  
 148 Kelbert et al (2008). Since some observatories locate near ocean, the ocean effect must  
 149 be taken into account, therefore the surface conductance in the resolution of  $1^\circ \times 1^\circ$  is  
 150 applied during the real data inversion.



151

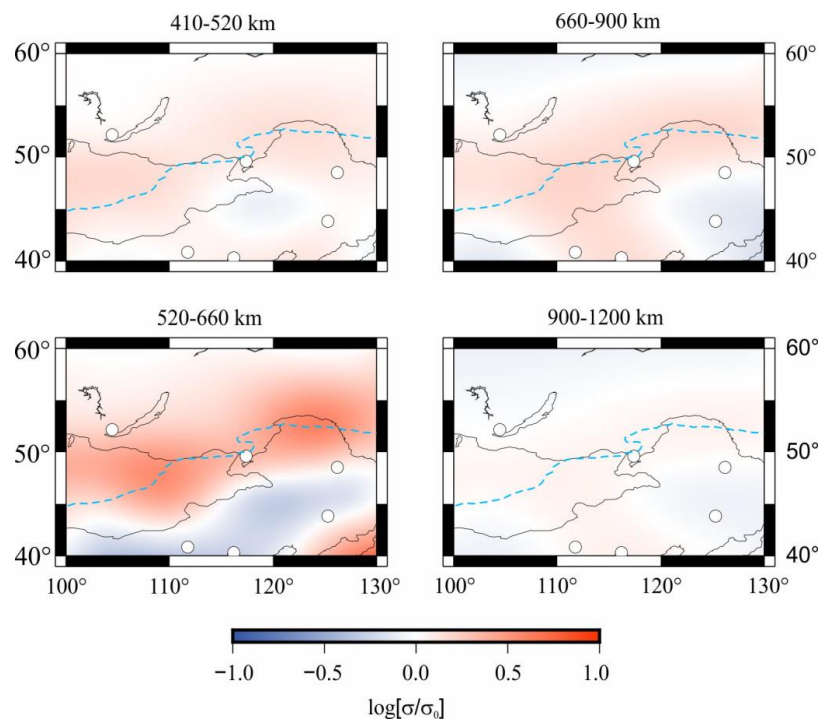
152 **Fig. 3.** Fitness curves of response of inversion results and the observed *C*-response for  
 153 three geomagnetic observatories distributed around the Mongol-Okhotsk suture. blue  
 154 lines are the inverted *C*-responses curves and the circles represent the observed *C*-  
 155 responses.

156 After 79 iterations, our inversion terminates with an RMS (Root Mean Square) of  
 157 1.18. The RMS at most stations falls in the range of 1.1-1.3. About 80% of stations have  
 158 RMS smaller than 1.4. The largest RMS is less than 1.7. This pattern of the RMS  
 159 distribution suggests that the *C*-responses on all the stations can be fitted quite well,  
 160 indicating that the inversion model is reliable. The fitting curves of typical observatories  
 161 are shown in Fig. 3. It can be seen that the inverted *C*-responses fit well with the  
 162 observed curves at most stations, especially at the short periods. As mentioned above,  
 163 we think the inversion result is reliable.

164 The electrical structure beneath Northeastern China and its adjacent areas at layers  
 165 of 410-520, 520-670, 670-900, 900-1200 km are plotted at Fig. 4. It can be seen that,  
 166 in the layer of 520-660 km, there are two continuous low resistivity anomaly bodies  
 167 distributed in a gourd shape along the Mongol-Okhotsk suture zone, and the scale of  
 168 the anomaly body is about  $10^{\circ} \times 20^{\circ}$ , the average conductivity of the anomaly body is  
 169 2S/m, while the conductivity of the center of the anomaly body can reach 7S/m, about  
 170 7 times higher than the global average value (Kelbert et al., 2009). The above sensitivity  
 171 tests can also explain the reliability of such large-scale electrical anomaly. To further  
 172 verify the reliability of the abnormal, after fixing the electrical values of the grid model



173 in the abnormal area at 520-660 km depth, we conducted inversion again. The new  
174 result showed that the RMS became larger, and high conductivity anomaly bodies  
175 appeared at the boundary of the fixed area, which can also indicate the reliability of the  
176 anomaly bodies in the target area.



177

178 **Figure 4.** Slices of the electrical conductivity at the depth of 410-520, 520-670,

179 670-900, 900-1200 km of the inverted 3-D model.

## 180 4. Discussion

### 181 4.1 Subduction range of the Western Pacific plate

182 Seismic images show that the subduction plate of the Western Pacific plate lies flat  
183 on the bottom of the mantle transition zone beneath East China, however, almost all the  
184 seismic imaging results reveals that the subduction front of the Pacific plate seems to  
185 be constrained to the east of the North-South Gravity Lineament (NSGL), and doesn't  
186 exceed the NSGL (Ma et al., 2019; Zhao et al, 2009). Therefore, the high conductivity  
187 abnormal seems to be independence with the subducted Pacific plate.





188 In addition, Yuan et al (2020) imaged the electrical resistivity structure in the depth  
189 range of 350-1200 km beneath China by inverting the frequency-dependent ratios of  
190 geomagnetic field component at a relatively dense network of geomagnetic  
191 observatories. Their results also show that the western front of the subducting Pacific  
192 plate in the MTZ roughly coincides with the abrupt change in the surface topography  
193 in eastern China. Zhang et al (2020) obtained high-quality *C*-responses from the dense  
194 geomagnetic observatories, and obtained the electrical structure of the MTZ of eastern  
195 China. To the east of NSGL, most geomagnetic observatories show high conductivity  
196 in MTZ; but for the observatories in the west of NSGL, the conductivity of most  
197 observatories is relatively low. However, Manzhouli (MZL) observatory, which is far  
198 away from NSGL shows obvious characteristics of high conductivity. This abnormal is  
199 inferred to be caused by the mantle plume under Siberia craton. Due to the limitation  
200 of 1-D inversion, it is difficult to show whether there is a connection between the high  
201 conductivity beneath MZL observatory and the high conductivity found in MTZ of  
202 eastern China.

203 Benefited from the realization of 3-D GDS inversion, several 3-D electrical  
204 structure models of global or local regions have been obtained. Since the limitation of  
205 the data density, most electrical models can only show that there is a high conductivity  
206 anomaly model in MTZ beneath east china, the resolution of the anomaly body is  
207 insufficient. Zhang et al (2022) used densely distributed observatories to obtain more  
208 accurate inversion result. The new obtained result show that the stagnant Pacific plate  
209 seems to be about 500 km away from NSGL. This may also indicate that the stagnant  
210 plate in the MTZ of eastern China and the high conductivity anomaly body in the area  
211 west of NSGL may have different formation mechanisms.

212 In summary, we concluded that the stagnant pacific plate could be constrained at  
213 the east of NSGL, corresponding to the high conductivity abnormal at the east of  
214 Songliao basin at the depth of 520-670 km as shown in Fig. 4. As for the high  
215 conductivity beneath Mongol-Okhotsk suture, it seen to be less affected by the Pacific  
216 tectonic domain.

#### 217 **4.2 Sources of Volcanic materials in GXAR**



218 A NE trending volcanic rock belt with a length of 1700 km and a width of 900 km  
219 is distributed in GXAR (Xu et al., 2013). Some researchers believe that magmatism in  
220 GXAR is induced by mantle plume (Lin et al., 1999). However, there is no evidence of  
221 earthquakes or He isotopes in the current research results indicating that there is a  
222 mantle plume under the Xing'an-Mongolia Orogenic Belt (Huang and Zhao, 2006;  
223 Chen et al., 2007). Isotopic dating has shown that the Early Cretaceous volcanic events  
224 in GXAR lasted at least 30 Ma, which is inconsistent with the rapid manner in which  
225 magma is formed in association with a mantle plume (Deng et al., 2019).

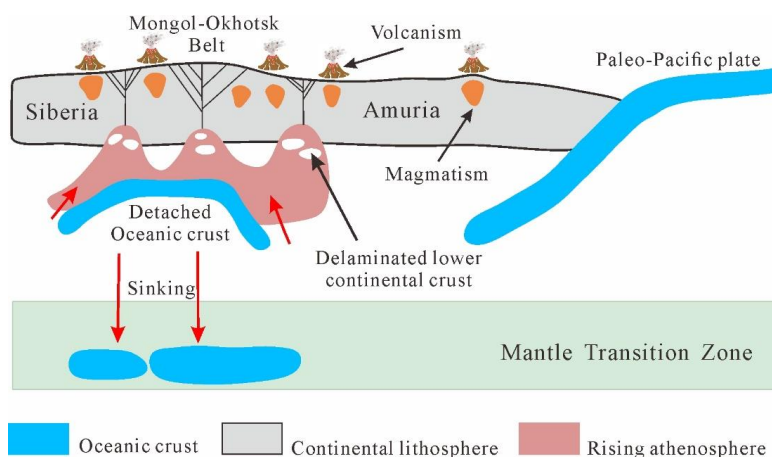
226 For the tectonic domain controlling the eruption, some scholars believe that it is  
227 mainly related to the retreat of the Pacific plate (Faure and Natalin, 1992; Zhang et al.,  
228 2010; Zhang et al., 2011; Ouyang et al., 2013, 2015). However, the temporal and spatial  
229 distribution characteristics of volcanic rocks and the paleotectonic environment do not  
230 support the above view (Engebretson et al., 1985; Maruyama and Seno, 1986; Kimura  
231 et al., 1990; Yarmolyuk and Kovalenko, 2001). Xu et al. (2013) pointed out that the  
232 Paleo Pacific tectonic domain mainly controls the magmatic and tectonic evolution in  
233 the east of Songliao Basin.

234 In recent years, more and more people believe that the late Mesozoic magmatic  
235 activity in the GXAR is related to the southward subduction of the Mongol-Okhotsk  
236 Ocean (Zorin, 1999; Meng, 2003; Ying et al., 2010). In space, the eruption of Early  
237 Cretaceous volcanic rocks in the northeast of GXAR was slightly later than that in the  
238 northwest, which may be related to the gradual closing process of the Mongol-Okhotsk  
239 Ocean from west to east (Cogné et al., 2005; Tomurtogoo et al., 2005; Metelkin et al.,  
240 2010; Sun et al., 2013; Yang et al., 2015a)

241 In combination with the above geological analysis and the acquisition of high  
242 conductivity anomaly bodies in the MTZ beneath the suture zone in this paper,. As  
243 shown in Fig. 5, we propose a hypothesis that the Okhotsk Ocean subducted to the north  
244 under the Siberian plate, and in the process of southward subduction, it subducted to  
245 the lower part of Northeast China, and the oceanic crust materials in the two-way small  
246 angle subduction entered the lower part of the land on both sides. Subsequently, the  
247 Okhotsk Ocean gradually closed in a scissors style from west to east, and the Okhotsk



248 Ocean disappeared, making the Siberian Craton and the North China Craton compress  
 249 and collide with each other to form the Mongol-Okhotsk suture zone. The oceanic crust  
 250 materials brought in by subduction carry a lot of water into the mantle. Under the deep  
 251 thermal action, the subduction materials with high water content and asthenosphere  
 252 materials produce partial melting, and migrate upward due to buoyancy. During the  
 253 transmission to the top of the lithosphere, when encountering the dry old and hard  
 254 lithosphere in the upper part, they can only appear in the form of continental basalt  
 255 magma from tectonic weak units such as plate suture zones. Therefore, a large number  
 256 of igneous rocks are distributed in the western margin of Songliao Basin and the eastern  
 257 side of Mongolia Okhotsk suture zone. The oceanic crust material gradually sinks over  
 258 time. When it migrates to the MTZ, it is blocked by a 660 km discontinuous interface,  
 259 and the oceanic crust material stops at the lower layer of the mantle transition zone.



260 **Fig. 5.** Geodynamic model of the deep structure beneath Northeast Asia.

261

## 262 **5. Conclusion**

263 In this paper, based on the dense geomagnetic observatories net-work and the 3-D  
 264 GDS inversion technique, the high precision electrical structure beneath northeast  
 265 China was obtained. A high conductive abnormal beneath the Mongol-Okhotsk suture  
 266 was found, which may cause the widely spread igneous rocks. The main conclusions  
 267 drawn as a result of this study are as follows:



268 (1) High resolution electrical conductivity in the MTZ of the Northeastern China  
269 was obtained basing on the dense geomagnetic data.

270 (2) The high conductor distributed in a gourd shape and parallel to the Mongol-  
271 Okhotsk suture may be related to the closure of the Okhotsk ocean.

272 (3) The high conductor beneath Mongol-Okhotsk suture was speculated as the  
273 subducted oceanic crust materials, it leads the volcanic events on the ground  
274 and sinking gradually at the bottom of the MTZ.

#### 275 **Authorship Contribution Statement**

276 Yanhui Zhang: Conceptualization, Methodology, Writing-review & editing.

277 Yuyan Zhang: Writing-original draft, Data curation. Yue Yang: Supervision,  
278 Investigation, Writing-review & editing. Longshuang Ma: Visualization, Software,  
279 Validation.

#### 280 **Declare of Conflicting Interest**

281 The authors declare that they have no known competing financial interests or  
282 personal relationships that could have appeared to influence the work reported in this  
283 paper.

#### 284 **Acknowledgments**

285 This work was supported by the National Natural Science Foundation of China  
286 (Grant 42104079 and 42074080) and the Natural Science Foundation of Hebei Province  
287 of China (Grant number D2021210007), to which we are very grateful. The authors  
288 would like to thank National Geomagnetic Network Center of China for providing the  
289 geomagnetic data. The inversion is developed on ModEM testbed. Some figures were  
290 prepared using GMT software (Wessel & Smith, 1998).

#### 291 **References**

- 292 1. Avdeev, D., Avdeeva, A., 2009. 3D magnetotelluric inversion using a limited-  
293 memory quasi-newton optimization. *Geophysics* 74 (3), F45–F57.
- 294 2. Chen, Y., Zhang, Y., Graham, D., Su, S., Deng, J., 2007. Geochemistry of Cenozoic  
295 basalts and mantle xenoliths in Northeast China. *Lithos*, 96, 108–126.



- 296 3. Cogné J P, Kravchisky V A, Halim N, et al., 2005. Late Jurassic-Early Cretaceous  
297 closure of the Mongol-Okhotsk Ocean demonstrated by new Meozoic  
298 palaeomagnetic results from the Trans-Baikal area (SE Siberia). *Geophysical*  
299 *Journal International*. 163:813-832.
- 300 4. Deng, C., Sun, D., Li, G., Lu, S., Tang, Z., Gou, J., Yang, Y., 2019. Early Cretaceous  
301 volcanic rocks in the Great Xing'an Range: Late effect of a flat-slab subduction.  
302 *Journal of Geodynamics*. 124(FEB.):38-51.
- 303 5. Egbert, G.D., Kelbert, A., 2012. Computational recipes for electromagnetic inverse  
304 problems. *Geophys. J. Int.* 189 (1), 251–267.
- 305 6. Eklblom, H., 1988. A new algorithm for the Huber estimator in linear models. *Bit*  
306 *Numerical Mathematics* 28 (1), 123–132.
- 307 7. Engebretson D C, Cox A, Gordon R G., 1985. Relative motions between oceanic  
308 and continental plates in the Pacific basin. *Geological Society of America, Special*  
309 *Paper*. 206:1-59.
- 310 8. Everett, M.E., Constable, S. & Constable, C.G., 2003. Effects of near-surface  
311 conductance on global satellite induction responses, *Geophys. J. Int.*, 153(1), 277–  
312 286.
- 313 9. Farquharson, G, C., 2008. Constructing piecewise-constant models in  
314 multidimensional minimum-structure inversions. *Geophysics* 73 (1), K1–K9.
- 315 10. Faure M., Natalin B., 1992. The geodynamic evolution of the eastern Eurasian  
316 margin in Mesozoic times. *Tectonophysics*. 208:397-411.
- 317 11. Gradstein, F., Ogg, J., Smith, A., Agterberg, F., Bleeker, W., Cooper, R., Davydov,  
318 V., Gibbard, P., Hinnov, L., House, M., 2004. *A Geologic Time Scale 2004*.  
319 Cambridge University Press, Cambridge.
- 320 12. Grayver, A. V., Munch, F. D., Kuvshinov, A., Khan, A., Sabaka, T. J., &  
321 Toffnerclausen, L., 2017. Joint inversion of satellite detected tidal and  
322 magnetospheric signals constrains electrical conductivity and water content of the  
323 upper mantle and transition zone. *Geophysical Research Letters*, 44(12), 6074–  
324 6081.
- 325 13. Halim, N., Kravchinsky, V., Gilder, S., Cogné J.-P., Alexyutin, M., Sorokin, A.,



- 326 Courtilot, V., Chen, Y., 1998. A palaeomagnetic study from the Mongol–Okhotsk  
327 region: rotated Early Cretaceous volcanics and remagnetized Mesozoic sediments.  
328 *Earth Planet. Sci. Lett.* 159, 133–145.
- 329 14. Huang, J., Zhao, D., 2006. High-resolution mantle tomography of China and  
330 surrounding regions. *J. Geophys. Res.* 111, B09305.
- 331 15. Kelbert, A., Egbert, G.D., Schultz, A., 2008. Non-linear conjugate gradient  
332 inversion for global EM induction: Resolution studies. *Geophys. J. Int.* 173 (2),  
333 365–381.
- 334 16. Kelbert, A., Schultz, A. & Egbert, G., 2009. Global electromagnetic induction  
335 constraints on transition-zone water content variations, *Nature*, 460, 1003–1007.
- 336 17. Kimura G, Takahashi M, Kono M., 1990. Mesozoic collision-extrusion tectonics  
337 in eastern Asia. *Tectonophysics.* 181(1-4):15-23.
- 338 18. Koch, S. & Kuvshinov, A., 2015. 3-D EM inversion of ground based geomagnetic  
339 Sq data. Results from the analysis of Australian array (AWAGS) data, *Geophys. J.*  
340 *Int.*, 200(3), 1284–1296.
- 341 19. Kuvshinov, A., 2012. Deep electromagnetic studies from land, sea, and space:  
342 progress status in the past 10 years. *Surv. Geophys.* 33 (1), 169–209.
- 343 20. Kuvshinov, A.V. & Olsen, N., 2006. A global model of mantle conductivity derived  
344 from 5 years of CHAMP, Ørsted, and SAC-C magnetic data. *Geophys. Res. Lett.*,  
345 33, L18301, doi:10.1029/2006GL027083.
- 346 21. Li, S., 2019. Global 3D imaging of electrical structure in mantle transition zone (in  
347 Chinese with English Abstract) PhD thesis, Jilin University.
- 348 22. Li, S., Weng, A, Zhang, Y, Schultz, A., Li, Y., & Tang, Y., et al., 2020. Evidence of  
349 bermuda hot and wet upwelling from novel three-dimensional global mantle  
350 electrical conductivity image. *Geochemistry, Geophysics, Geosystems*, 21(6).
- 351 23. Lin, Q., Ge, W., Sun, D., Wu, F., 1999. Geomechanical significance of the  
352 Mesozoic volcanics in Northeast Asia, *Chinese Journal of Geophysics.* 42, 75-84.
- 353 24. Ma, J., Tian, Y., Liu, C., Zhao, D., Feng, X., Zhu, H., 2018. P-wave tomography of  
354 northeast asia: constraints on the western pacific plate subduction and mantle  
355 dynamics. *Physics of the earth and planetary interiors.* 274, 105-126.



- 356 25. Maruyama M, Seno T., 1986. Orogeny and relative plate motions: Example of the  
357 Japanese Islands. *Tectonophysics*. 127(3-4):305-329.
- 358 26. Meng Q R., 2003. What drove late Mesozoic extension of the northern China-  
359 Mongolia tract? *Tectonophysics*. 369:155-174.
- 360 27. Metelkin D V., Vernikovsky V A., Kazansky A Y., et al., 2010. Late Mesozoic  
361 tectonics of Central Asia based on paleomagnetic evidence. *Gondwana Research*.  
362 18: 400-419.
- 363 28. Munch, F.D., Grayver, A.V., Kuvshinov, A.V. & Khan, A., 2017. Stochastic  
364 inversion of geomagnetic observatory data including rigorous treatment of the  
365 ocean induction effect with implications for transition zone water content and  
366 thermal structure, *J. geophys Res.*, 123, 31–51.
- 367 29. Nocedal, J.&Wright, S.J., 1999. *Numerical Optimization*, 2nd edn, Springer.
- 368 30. Ouyang H G, Mao J W, Santosh M, et al., 2013. Geodynamic setting of Mesozoic  
369 magmatism in NE China and surrounding regions: perspectives from spatio-  
370 temporal distribution patterns of ore deposits. *Journal of Asian Earth Sciences*.  
371 78:222-236.
- 372 31. Ouyang H G., Mao J W., Zhou Z H., et al., 2015. Late Mesozoic metallogeny and  
373 intracontinental magmatism, southern Great Xing'an Range, northeastern China.  
374 *Gondwana Research*. 27:1153-1172.
- 375 32. Püthe, C. & Kuvshinov, A., 2014. Mapping 3-D mantle electrical conductivity from  
376 space: a new 3-D inversion scheme based on analysis of matrix Q-responses,  
377 *Geophys. J. Int.*, 197(2), 768–784.
- 378 33. Semenov, A. & Kuvshinov, A., 2012. Global 3-D imaging of mantle conductivity  
379 based on inversion of observatory C-responses-II. Data analysis and results,  
380 *Geophys. J. Int.*, 191(3), 965–992.
- 381 34. Sun D Y, Gou J, Wang T H, et al., 2013. Geochronological and geochemical  
382 constraints on the Erguna massif basement, NE China-subduction history of the  
383 Mongol–Okhotsk oceanic crust. *International Geology Review*. 55 (14):1801-1816.
- 384 35. Tang J, Xu W L, Wang F, et al., 2015. Geochronology, geochemistry, and  
385 deformation history of late Jurassic-Early Cretaceous intrusive rocks in the Erguna



- 386 Massif, NE China: Constraints on the late Mesozoic tectonic evolution of the  
387 Mongol-Okhotsk orogenic belt. *Tectonophysics*. 658:91-110.
- 388 36. Tomurtogoo O, Windley B F, Kröner A, et al., 2005. Zircon age and occurrence of  
389 the Adaatsag ophiolite and Muron shear zone, central Mongolia: constraints on the  
390 evolution of the Mongol-Okhotsk ocean, suture and orogen. *Journal of the*  
391 *Geological Society, London*. 162:125-134.
- 392 37. Tomurtogoo, O., Windley, B. F., Kroner, A., Badarch, G., & Liu, D. Y., 2005.  
393 Zircon age and occurrence of the adaatsag ophiolite and muron shear zone, central  
394 mongolia: constraints on the evolution of the mongol-okhotsk ocean, suture and  
395 orogen. *Journal of the Geological Societ*. 162(1), 197-229.
- 396 38. Utada, H., Koyama, T., Obayashi, M. & Fukao, Y., 2009. A joint interpretation of  
397 electromagnetic and seismic tomography models suggests the mantle transition  
398 zone below Europe is dry, *Earth planet. Sci. Lett.* 281(3), 249–257.
- 399 39. Uyeshima, M. & Schultz, A., 2000. Geoelectromagnetic induction in a  
400 heterogeneous sphere: a new three-dimensional forward solver using a  
401 conservative staggered-grid finite difference method. *Geophys. J. Int.*, 140(3),  
402 636–650.
- 403 40. Weng, A.H., Li, D.J., Li, Y.B., Li, S.R., Yang, D.F., Yang, Y. & Liu, Y.H., 2015.  
404 Selection of parameter types in controlled source electromagnetic method, *Chin. J.*  
405 *Geophys.* 58(2), 697–708(in Chinese).
- 406 41. Wessel, P., Smith, W., 1998. New, improved version of Generic Mapping Tools  
407 released, *EOS, Trans. Am. geophys. Un.* 79, 579.
- 408 42. Xu, W., Pei, F., Feng, W., Meng, E., Ji, W., Yang, D., Wang, W., 2013. Spatial–  
409 temporal relationships of Mesozoic volcanic rocks in NE China: Constraints on  
410 tectonic overprinting and transformations between multiple tectonic regimes.  
411 *Journal of Asian Earth Sciences*. 74(sep.25):167-193.
- 412 43. Yang, Y T, Guo Z X, Song C C, et al.,2015 A short-lived but significant Mongol-  
413 Okhotsk collisional orogeny in latest Jurassic-earliest Cretaceous. *Gondwana*  
414 *Research*. 28:1096-1116.
- 415 44. Yarmolyuk V V., Kovalenko V I., 2001. The Mesozoic-Cainozoic of Mongolia. In:





- 416 Dergunov, A. B., ed., Tectonics, magmatism, and metallogeny of Mongolia.  
417 Taylor& Francis Group, London. 203-244.
- 418 45. Ying J F, Zhou X H, Zhang L C, et al., 2010. Geochronological framework of  
419 Mesozoic volcanic rocks in the Great Xing'an range, NE China, and their  
420 geodynamic implications. *Journal of Asian Earth Sciences*. 39:786-793.
- 421 46. Yuan, Y., Uyeshima, M., Huang, Q., Tang, J., Li, Q., 2020. Continental-scale deep  
422 electrical resistivity structure beneath China. *Tectonophysics* 790.
- 423 47. Zhang F Q, Chen H L, Yu X, et al., 2011. Early Cretaceous volcanism in northern  
424 Songliao Basin, NE China, and its geodynamic implication. *Gondwana Research*.  
425 19:163-176.
- 426 48. Zhang J H, Gao S, Ge W C, et al., 2010. Geochronology of the Mesozoic volcanic  
427 rocks in the Great Xing'an Range, northeastern China: implications for subduction-  
428 induced delamination. *Chemical Geology*. 276:144-165.
- 429 49. Zhang, Y., Weng, A., Li, S., Yang, Y., Tang, Y., Liu, Y., 2020. Electrical conductivity  
430 in the mantle transition zone beneath Eastern China derived from L1-Norm C-  
431 responses. *Geophys. J. Int.* 221 (2), 1110–1124.
- 432 50. Zhang, Y.; Yang, Y., 2022. Three-dimensional inversion resolution in detecting  
433 stagnant slabs using a dense geomagnetic depth sounding method, *Physics of the*  
434 *earth and planetary interiors*.
- 435 51. Zhao, D., Tian, Y., Lei, J., Liu, L., Zheng, S., 2009. Seismic image and origin of  
436 the Changbai intraslab volcano in East Asia: Role of big mantle wedge above the  
437 stagnant Pacific slab. *Phys. Earth Planet. Inter.* 173 (3), 197–206.
- 438 52. Zhao, X., Coe, R.S., Zhou, Y., Wu, H., Wang, J., 1990. New paleomagnetic results  
439 from northern China: collision and suturing with Siberia and Kazakhstan. *Tectono-*  
440 *physics* 181, 43–81.
- 441 53. Zonenshain, L.P., Kuzmin, M.I., Natapov, L.M., 1990. *Geology of the USSR: a*  
442 *Plate–Tectonic Synthesis*. American Geophysical Union *Geodyn. Ser.*, vol.21. 242  
443 pp. Ch. 7.
- 444 54. Zorin, Y.A., 1999. Geodynamics of the western part of the Mongolia–Okhotsk col-  
445 lisional belt, Trans-Baikal region (Russia) and Mongolia. *Tectonophysics* 306, 33–

<https://doi.org/10.5194/egusphere-2023-480>

Preprint. Discussion started: 24 March 2023

© Author(s) 2023. CC BY 4.0 License.



446      56.

447